Robofurnace: A semi-automated laboratory chemical vapor deposition system for high-throughput nanomaterial synthesis and process discovery

C. Ryan Oliver, William Westrick, Jeremy Koehler, Anna Brieland-Shoultz, Ilias Anagnostopoulos-Politis et al.

Additional information on Rev. Sci. Instrum.

Robofurnace: A semi-automated laboratory chemical vapor deposition system for high-throughput nanomaterial synthesis and process discovery

C. Ryan Oliver,[1] William Westrick,[1] Jeremy Koehler,[1] Anna Brieland-Shoultz,[1] Ilias Anagnostopoulos-Politis,[1] Tizoc Cruz-Gonzalez,[1] and A. John Hart[1,2,a)]

[1]*Department of Mechanical Engineering, University of Michigan, Ann Arbor, Michigan 48109, USA*
[2]*Department of Mechanical Engineering, Massachusetts Institute of Technology, Cambridge, Massachusetts 02139, USA*

Laboratory research and development on new materials, such as nanostructured thin films, often utilizes manual equipment such as tube furnaces due to its relatively low cost and ease of setup. However, these systems can be prone to inconsistent outcomes due to variations in standard operating procedures and limitations in performance such as heating and cooling rates restrict the parameter space that can be explored. Perhaps more importantly, maximization of research throughput and the successful and efficient translation of materials processing knowledge to production-scale systems, relies on the attainment of consistent outcomes. In response to this need, we present a semi-automated lab-scale chemical vapor deposition (CVD) furnace system, called "Robofurnace." Robofurnace is an automated CVD system built around a standard tube furnace, which automates sample insertion and removal and uses motion of the furnace to achieve rapid heating and cooling. The system has a 10-sample magazine and motorized transfer arm, which isolates the samples from the lab atmosphere and enables highly repeatable placement of the sample within the tube. The system is designed to enable continuous operation of the CVD reactor, with asynchronous loading/unloading of samples. To demonstrate its performance, Robofurnace is used to develop a rapid CVD recipe for carbon nanotube (CNT) forest growth, achieving a 10-fold improvement in CNT forest mass density compared to a benchmark recipe using a manual tube furnace. In the long run, multiple systems like Robofurnace may be linked to share data among laboratories by methods such as Twitter. Our hope is Robofurnace and like automation will enable machine learning to optimize and discover relationships in complex material synthesis processes. © *2013 AIP Publishing LLC*. [http://dx.doi.org/10.1063/1.4826275]

I. INTRODUCTION

Materials research is nearing a frontier where synergetic advances in computation and automation will enable rapid discovery and deployment of materials with novel properties.[1,2] However, most development of new materials still relies on educated yet empirical experimentation with synthesis recipes. This process, which consumes significant time and money, is often manual and involves exploration of a limited portion of a very large parameter space.

For example, a frenzy of research activity has focused on synthesis of carbon nanotubes (CNTs) and graphene, because these nanostructures exhibit outstanding mechanical, electrical, thermal, and optical properties,[3–9] and could enable novel bulk materials. However, integration of these and other nanostructured materials into commercial products has been limited by the rate at which laboratory demonstrations can be validated for commercial production with quality control.[10,11] Chemical vapor deposition (CVD), which is the dominant method of fabricating CNT and graphene films, is exquisitely sensitive to sometimes unknown fluctuations in process conditions: influences from the ambient lab conditions such as humidity and variability in research operating procedures.[12]

Moreover, the large number of process parameters, including substrate material, temperature, gas composition, and flow rate, means that even local optimization of results takes extensive time and effort.

Within academia, laboratories working on new materials often resort to manual processing tools (e.g., small tube furnaces), which may be built from scratch or carried over from previous projects. In the authors' opinion, ubiquitous use of manual tube furnaces for CVD materials research in laboratories limits the rate of materials synthesis experimentation and contributes to the purported problem of outcome variability. What other options do we have as researchers? Cleanrooms are typically geared toward processing on full wafers, using equipment that is very expensive and therefore creates a high barrier to entry. This barrier exists for university researchers who want to build a new material or device, as well for small business and most large companies. For most companies that need to utilize microfabrication, the ultimate choice is to contract a foundry to use a standard process, because it is financially prohibitive to buy dedicated processing tools. And, in many cases, processing of small samples rather than full wafers can improve throughput of development, at low cost, assuming the processing tools do not compromise the conditions of the processing environment. Therefore, we hypothesized that an automated CVD system that is specifically designed to handle centimeter-scale substrate samples would be

---

a)Author to whom correspondence should be addressed. Electronic mail: ajhart@mit.edu. Tel.: 617 324 7022.

a potentially disruptive approach to increasing the throughput of lab experimentation in materials synthesis.

Nowadays, the development of new lab-scale automation can leverage the increasing availability and affordability of modular electromechanical systems and software. The first fully automated artificial intelligence system for scientific discovery, called Dendral, was developed in the 1960s.[13–15] Dendral used a heuristic search algorithm to analyze mass spectroscopy data to determine the chemical structure of a sample. Remarkably, although automation has become increasingly important in the scientific process, the application of automated systems has been limited to a few disciplines. For example, high speed combinatorial systems have proven useful in complex sample spaces such as DNA sequencing and microhotplates for chemical sensing.[16,17]

We present Robofurnace, a semi-automated lab scale CVD system for high throughput synthesis of thin films and its application to development of improved processes for carbon nanotube (CNT) growth. Robofurnace is built around a standard tube furnace, automates sample insertion and removal, and uses motion of the furnace combined with heater power control to achieve rapid heating and cooling of the sample. The system has a 10-sample magazine and motorized transfer arm, which isolates the samples from the lab atmosphere and enables highly repeatable placement of the sample within the reactor tube. The system enables automated continuous operation of the CVD reactor, with asynchronous loading/unloading of samples. We demonstrate the use of Robofurnace in an exemplary study of CNT forest growth and discuss the role automation plays in controlling variation between experiments. Last, we demonstrate how Robofurnace enabled discovery of a rapid CVD recipe for CNT forest growth, which resulted in a 10-fold higher mass density than a benchmark recipe using a manual tube furnace.

II. SYSTEM DESIGN AND CONSTRUCTION

A. Overview and specifications

Robofurnace is a tabletop system built using primarily off-the-shelf components and integrated using a modular aluminum frame system, which is reconfigurable and provides structural support and precision alignment. The system is described with reference to the modules labeled in Figure 1 and detailed below.

- Tube furnace. A tube furnace (Thermo-Fisher Minimite) is mounted on aluminum frame rails, which act as linear guides for a motion system that enables the furnace to move along the length of the reactor tube. The furnace has a 300 mm heated region, integrated PID temperature controller, and is fitted with a fused quartz tube.
- Magazine. The magazine has compliant slots for each of 10 sample "boats" (75 × 20 mm), which are made from silicon wafers and etched with sample alignment features. The magazine is enclosed in a stainless steel chamber, made using an extruded box section; this is called the sample load/lock chamber. The chamber is accessed via a hinged door and is isolated from the transfer arm and CVD system to enable purging.
- Transfer arm. A custom quartz transfer arm (Figure S2 in the supplementary material[20]), attached to a single-axis vertical stage and linear slide, transports boats from the magazine to the reactor tube. The transfer arm is enclosed in bellows attached to the magazine chamber to maintain a clean atmosphere within the system.
- Gas delivery system. The gas delivery system is comprised of 4–10 digital mass flow controllers (Alborg FMA 5500), which connect the tank regulators to the
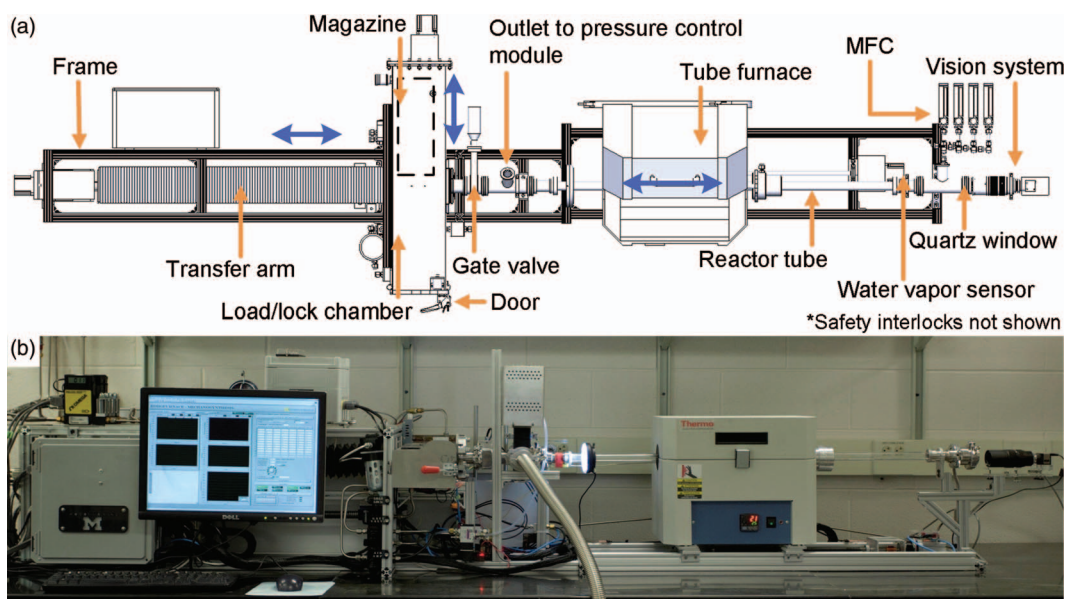
FIG. 1. Robofurnace automated CVD system. (a) Top-view schematic showing the major subsystems. Blue lines, from left to right, represent motion of the transfer arm, sample magazine, and tube furnace. (b) Photograph of prototype Robofurnace on a standard laboratory bench, including LabVIEW software interface. The system is ~9 feet wide and 2.5 feet deep.

inlet of the reactor; all the output lines merge to a single line before the reactor entry.

- Pressure control system. Robofurnace can be configured for atmospheric pressure or vacuum operation by switching the reactor exhaust between a bubbler and a vacuum system. The vacuum system consists of a vacuum pump (Varian DS 302), Micro Pirani transducer (MKS R750C) to measure absolute pressure and a closed loop butterfly valve (MKS 153D). The butterfly valve is located between the outlet of the reactor tube and the vacuum pump. A pneumatic gate valve (Kurt J. Lesker SG0150PVQF) separates the reactor tube and sample load/lock that is only opened during loading and unloading of the reactor. All vacuum connections are based on industry standardized ISO 40 vacuum compatible connections.

- Water vapor control system. A downstream hygrometer (Khan Cermet II) is used to measure the water vapor within the system and has a bypass to prevent contamination. A tank of 0.5% O_2 in He is connected to one of the MFCs, enabling addition of this gas which reacts with H_2 in the heated zone of the reactor to create a controlled amount of water vapor between 50 and 10 000 ppm (Figure S3 in the supplementary material[20]).[12, 18]

- Vision system. A digital video camera (described later) is focused down the axis of the reactor tube and is used to measure the film thickness using a computer vision algorithm.

- Safety interlocks and gas detection system. A hydrogen sensor (Neodym HydroKnowz) mounted outside the door of the load/lock activates a relay that cuts power to the furnace and stops the gas flows upstream by closing solenoids. The sensor minimum sensitivity threshold is 100 ppm. Limit switches and contact switches keep the system from moving when being loaded or unloaded.

- Software. A custom-built LabView program controls all system operations and interfaces with the hardware via data acquisition cards (NI-6008) located within the control box. During each experiment the software records the processing parameters and *in situ* metrology data. After each experiment, the software posts the data file to dropbox and to a webserver (http://www.robofurnace.com). The results are also shared via twitter to #robofurnace.

Robofurnace was designed to meet the specifications in Table I. The rapid heating and cooling rates enable prototyping of conditions that are amenable to continuous roll-to-roll processing, as well as spatial and temporal control of gas decomposition upstream of the substrate. The maximum error in heating and cooling rates is a measurement of the maximum deviation in the temperature of the sample when compared to a specified cooling rate. The maximum error rate of 10 °C ensures that reactions that are temperature sensitive can be performed within allowable limits. Repeatability of the sample placement along the reactor tube ensures that samples processed under an identical recipe are exposed to the same con-

TABLE I. System specifications.

Specification	Value
Sample heating rate	1–340 °C/min
Sample cooling rate	1–300 °C/min
Maximum furnace temperature	1100 °C
Maximum error in heating/cooling rate	±10 °C/min
Load/Unload time	15 min
Repeatability of sample placement along tube	±200 μm
Vision resolution	±20 μm
Minimum baseline moisture level	5 ppm

ditions within the reactor. The vision system resolution was determined by the need to measure thickness of carbon CNT thin films *in situ*. Finally, the ability to reduce moisture levels to a minimum (5 ppm) improves robustness and controls contamination of moisture sensitive samples.[10, 12] This target was chosen based on experience with CNT reactions, which are sensitive to reactor moisture levels of 100 ppm.

B. Detailed description of key modules

1. Motion systems

Robofurnace has three motion systems: the magazine, the transfer arm, and the furnace (Table II). The main purpose of the magazine motion system is to position the substrate sample with respect to the arm so it can pick up the boat and insert it into the furnace. A motor interfaced via a feedthrough in the magazine case moves the magazine in the direction perpendicular to the furnace tube. This motion positions the desired boat in the insertion path, where it can be accessed by the transfer arm moving along the tube axis, or for the researcher to load/unload samples. When that magazine is fully ejected the researcher can manually extend it further on telescopic rails to access all of the load positions in the magazine.

The transfer arm motion system moves the arm along the axis defined by the quartz tube, enabling pick-and-place manipulation of the sample (boat) from the magazine into the furnace tube (Figure 2(b)). The high repeatability (±0.25 mm) specification of this motion system is required to place the sample at the desired location within the quartz tube. The arm has a second axis of motion to enable lifting and lowering the transfer arm.

The furnace motion system moves the furnace to enable wide-range control of the sample heating and cooling rate. The temperature of the furnace varies greatly along its length (Figure S4 in the supplementary material[20]). The temperature has a parabolic profile within the length of the heating coil,

TABLE II. Motion system specifications.

	Travel (mm)	Speed (mm/min)	Precision (mm)	Repeatability (mm)
Magazine	355	318	±1.25	±0.25
Transfer arm	762	1524	±1.25	±0.25
Furnace	305	1524	±1.25	±0.25
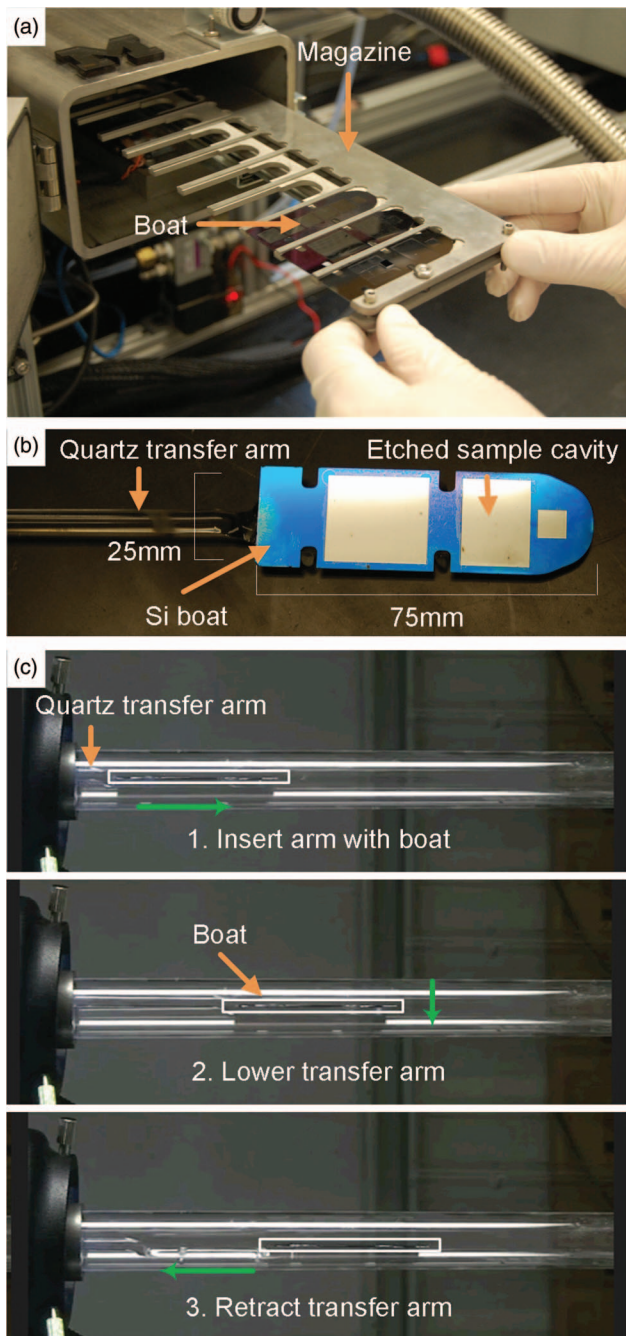
FIG. 2. Magazine and transfer arm sample load sequence. (a) Magazine in the extended position for loading of samples. (b) Single etched Si sample holder ("boat") resting on the quartz transfer arm. (c) Motion sequence where the transfer arm places a boat (holding substrate samples) in the reactor tube. The transfer arm enters the tube, then lowers, and retracts, leaving the boat in the tube.

and a rapid drop outside of this. Assuming the sample temperature is nearly identical to the surrounding furnace temperature based on its small mass allows the sample temperature to be controlled by the furnace position. Due to the steep change in temperature along the length of the furnace, a relatively high resolution was required (<1 mm). Based on the requirements of the magazine system, a Uni-Slide system (Velmex) was used to move the furnace. The system has a travel of 406 mm and uses a lead screw with a lead of 1.57 turns/mm, coupled to a stepper motor with 1.8 °/step.

TABLE III. Motion systems calculated torque and resolution values.

Motion system	Torque (N·m)	Resolution (μm/step)
Furnace	0.143	13
Arm	0.172	25

Both the arm and furnace motion systems were constructed using lead screws driven by stepper motors. The lead screw diameters and pitches were determined using standard design charts, resulting in a $\frac{1}{2}$ in.-10 screws for the furnace motion system and a 1in.-5 screw for the arm motion system. The calculated torque and single micro-step resolution from the two systems is given in Table III, and these values meet the system's speed requirements. The furnace motion system produces calculated torque of 143 N·m with a resolution of 13 μm/step and the transfer arm produces 0.17 N·m with a resolution of 25 μm/step. This was used to calculate a maximum speed of 1524 mm/min for both motion systems. The diameter of the transfer arm leadscrew was chosen to result in negligible deflection of the lead screw under its self-weight.

2. Magazine

The magazine (Figure 2(a)) is made of stainless steel to reduce moisture retention. It is mounted to a telescoping support, which is mounted to the magazine motion system. The telescoping support allows the researcher to withdraw the magazine to access each of the 10 sample "boats" for loading/unloading samples. The magazine has two main parts: the base for mounting to the motion system and a fixture for holding the boats (Figure 2(a)). To align the magazine to the transfer arm's axis of motion it is mounted to the base via a spring-loaded kinematic coupling. Bolts at each corner of the magazine are used to adjust the coupling and, therefore, align the magazine with the transfer arm. This motion system's lead screw is within the load/lock chamber and is connected to the motor via a vacuum-compatible rotary feedthrough. The boat (Figure 2(b)) is dimensioned to fit into a recess in the magazine, with three-point contact to ensure accurate placement (Figure 2(a)). The recess has an opening that supports the boat but allows the flat end of the transfer arm to approach underneath the boat and pick it up for insertion into the reactor tube.

3. Transfer arm

The transfer arm (Figure S2 in the supplementary material[20]) is used to pick-and-place the boat (with sample) from the magazine to the reactor tube. The transfer arm is a quartz rod (5 mm diameter, 600 mm length) with a flat rectangular fixture (50 × 10 × 3 mm) fused to one end. The rectangular fixture has four teeth that mate with notched silicon boats to prevent misalignment caused by motion-induced vibration or friction. The dimensions of the rectangular fixture are based on geometric constraints determined by the 25.4 mm reactor inner tube diameter. When a sample is placed inside the reactor tube, it is supported by the edges of the boat,

which rest against the tube walls. The teeth are only 2 mm tall so that the fixture in motion does not interfere with the boat at rest against the tube wall.

The quartz arm is mounted to the transfer arm motion system by a two-part clamp with a v-groove; the v-groove aligns the rod with the motion system. The transfer arm support is affixed to a z-stage, allowing the arm to lift and place boats. The z-stage is mounted to a linear motion system aligned to the reactor tube. Bellows connect the anchored end of the transfer arm to the load/lock chamber, enabling motion while isolating the transfer arm from the lab ambient.

4. Vision system

Robofurnace is equipped with a vision system, shown in Figure 3(a), to monitor the orientation of the sample in the tube and to measure the film thickness in real time. The specifications of this system were suited to millimeter-scale CNT forest growth; however, other optical methods and magnification parameters could be adopted using the same configuration. The camera (Edmund Optics, #EO-10012C) provides 10 megapixel color video of the sample through a quartz viewport attached to the reactor tube with a KF-40 flange. The camera is attached to a C-mount fixed focal length lens extender (2X magnification, Edmund Optics NT54-356) and a 75 mm focusable double gauss lens (Edmund Optics NT54-691). This arrangement allows a very long working distance (635 mm) with the desired field of view (FOV) (25 mm). The maximum full-resolution sampling rate of the camera is 2 Hz, which is sufficient for monitoring CNT forest growth.

To select the components of the vision system (Figure 3(b)), the primary magnification (M) was calculated to be $0.25\times$ by dividing the desired FOV, 6.4 mm, by the sensor width of 25.4 mm. The camera resolution (C_r) is equal to the pixel size of the sensor or 1.67 μm. Now, according to Eq. (1), the resolving power (S_r) of the camera and optics is 6.7 μm,

$$S_r = \frac{C_r}{M} = \frac{1.67}{0.25} = 6.7\,\mu\text{m}. \quad (1)$$

Accounting for 30% pixel size loss for the color CCD, the true resolving power is 8.7 μm. In other words, displacement of 8.7 μm at the focal point results in one pixel of displacement on the CCD:
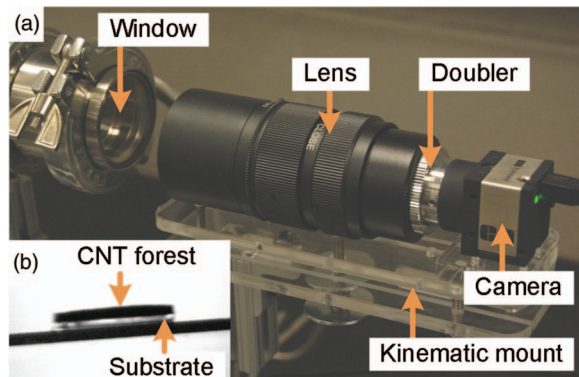
$$S_a(\mu\text{m}) = \frac{C_r 0.7}{M} = 8.7\,\mu\text{m}. \quad (2)$$

The next requirement was to choose a focal length that would achieve our desired magnification of $0.25\times$ when the distance, d_o, from the object (sample) to the lens is 635 mm. Via Eq. (3), the focal length required can be calculated as 211.5 mm:

$$f = \frac{d_o M}{M - 1}. \quad (3)$$

We selected a 75 mm lens and a focal length lens extender to achieve 150 mm focal length. Therefore, the real magnification was $0.3\times$.

From the selected lens a better description of resolution is equal to the line pair of the system, which is equal to twice the system resolution or 17.4 μm. According to the manufacturer's MTF function, the lens in the system has a resolution of 100 lp/mm at 50% contrast at an aperture of F4. Using the system at F8, due to the doubler, we expect the lens to be matched to the line pair resolution of the system, equaling $\sim$20 μm.

Last, based on the known FOV, magnification, and additional values given in Table IV, the depth of field (DOF) was calculated to be 26 mm,[19]

$$DOF = \frac{2sNcf^2(s - f)}{((f^4) - ((Nc(s - f))^2)} = \pm 26\,\text{mm}. \quad (4)$$

The depth of field is small relative to the boat length of 76 mm. Therefore, samples positioned within 26 mm of the focal plane are considered in focus and measurable. As shown later, the positioning accuracy of the pick-and-place system far exceeds this specification.

5. Software

The Robofurnace user interface and back-end automation routines were programmed in LabVIEW™. The back-end automation routines control Robofurnace (hardware and software) by a two-queued state machine architecture (Figure 4). A state machine is a system in which the next action taken by a system is determined by the state of an input. The first state machine (Event processing loop) controls the current experiment, i.e., stepping through the recipe and providing instructions to the respective parts of Robofurnace according to the input queue. The second state machine (Event producer loop) monitors the interface with the researcher, alarms, and sensors.

The interface, shown in Figure 5, has 3 display modules. The top left side of the display is the module for "Real-time

FIG. 3. Vision system. (a) Photograph of the vision system looking down the central axis of the reactor tube. (b) Image of a CNT forest during growth as taken by the vision system.

TABLE IV. Parameter values for depth of field analysis.

Constants	Description	Value
s	Subject distance	635 mm
N	f/number of the system	F8
c	Sensor circle of confusion	0.1393 mm
f	Focal length of the lens	162.5 mm
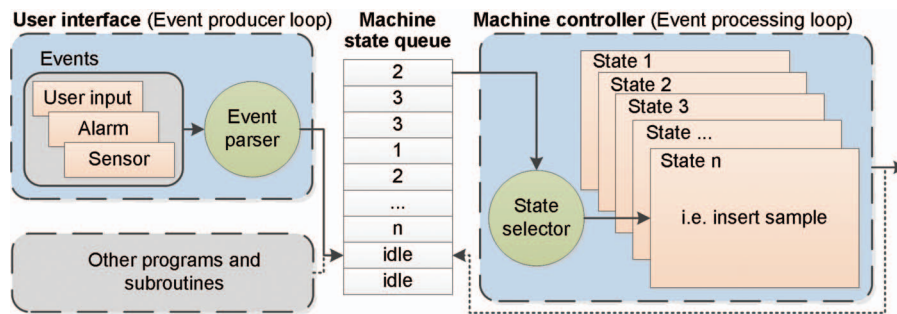
FIG. 4. Queued state machine architecture implemented using LabVIEW. User inputs, alarms, and sensors can generate events that are inserted into the queue. The machine controller loop then reads from the top of the queue and executes that action/event. Alarms are inserted to the top of the queue for immediate execution.

data." This module is comprised of six graphical panels, and this data is displayed in real time and saved to the data log for the experiment.

Using top right module, entitled "Real time process and metrology data," the researcher can enter in parameters (the "recipe") for an experiment. Parameters defined by the researcher include gas flows, furnace temperature, reactor pressure, and furnace position relative to the sample for each time step of the experiment. After entering in the desired recipe, a prompt is given for the researcher to input the sample location (boat) in the magazine. When entry is complete, the researcher can save the recipe into the recipe queue. Each researcher's name is linked to his or her email address so that

a notification, and a link to the process data, will be sent to the researcher upon completion of the experiment. The user can also configure the vision system to stop the experiment if the thickness of the film exceeds a specified value and/or can choose a rate in °C/s to cool the sample after the experiment.

At the bottom right of the researcher interface is a module entitled "System status" which notifies the researcher if a sensor listed in Table III has changed states. The sensor state variables are:

- **GV**: Indicates if the gate valve is open or closed.
- **Door**: Indicates if the load/lock door is open or closed.
- **Door Lock**: Indicates if the load/lock door is locked.

FIG. 5. LabVIEW software interface to Robofurnace, with recipe entry interface, real-time process data, and system status.
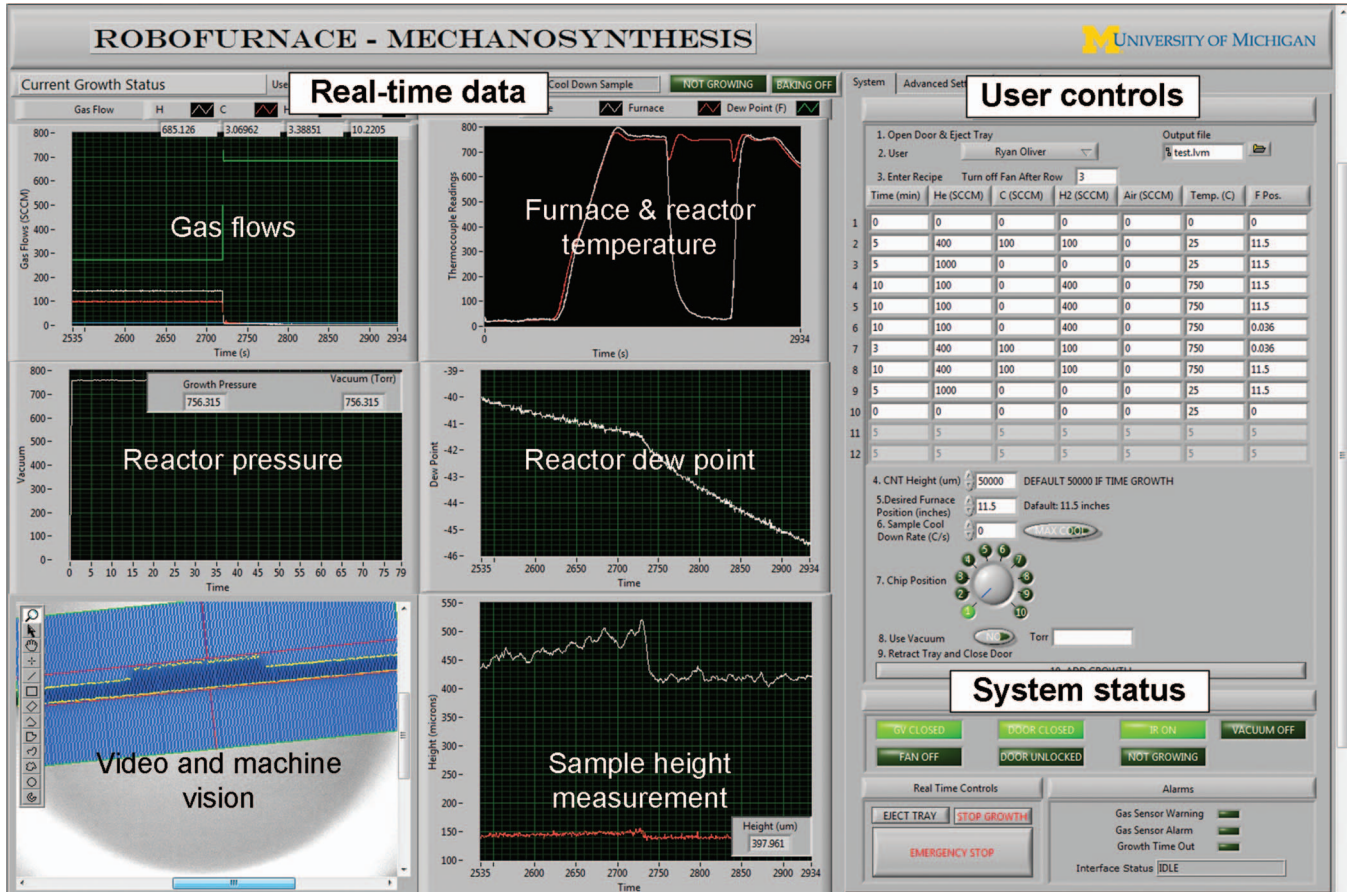
- **IR**: Indicates if the infrared sensor detects a sample in the magazine during insertion and removal for the current experiment.
- **Vacuum:** Indicates if the pressure system is active and the vacuum pump is on.
- **Fan:** Indicates if the cooling fan is on or off.
- **Not Growing:** Indicates if an experiment is being performed.

Alarms from the H_2 gas sensor are displayed at the bottom right of the system status module. The first alarm is a warning for a low level leak (4000 ppm); the second alarm is a high level alarm (20 000 ppm) that turns off furnace power, stops all motion, and closes MFC solenoids for each gas except the purging gas. There is a maximum time for each experiment, which, if exceeded, will show an alarm and shut the system down, presuming there was a malfunction. The last item in this module shows the current status of the queued state machine, which nominally displays IDLE. During a particular step in the process this indicator will change, for example, it may display "Moving magazine" to indicate the magazine motion system is active.

6. Furnace motion controller

With a stationary tube furnace as in traditional CVD systems, the maximum rates of heating and cooling are limited by the rate of power output by the heating coil and the thermal

mass of the furnace. Using Robofurnace, moving the furnace in addition to controlling the power delivered to the heating coil enables full range control of the heating and cooling rates, up to a maximum rate limited only by the thermal mass of the tube and the sample. For example, the sample can be heated and cooled very quickly by translating the furnace with respect to the sample, with the furnace maintained at a constant temperature.

To design the furnace motion controller to achieve this new capability, we developed a thermal model of the furnace based on temperature measurements (Figure S4 in the supplementary material[20]) taken at 1 cm intervals along the axis of the furnace tube. Equation (5) was fit to this data and used as an approximation of the temperature distribution for the controller design. In this equation, x is the distance from the sample to the center of the furnace, x_{max} is the distance from the center to the edge of the furnace, $T_{ambient}$ is the ambient room temperature, and T_{center} is the temperature at the center of the furnace (ideally, equal to the setpoint):

$$T(x) = (T_{center} - T_{ambient})\, erfc\left(\left[\frac{x}{1.5x_{max}}\right]^2\right) + T_{ambient}.$$

(5)

We assumed that radiation is the dominant heat transfer mechanism between the furnace (heating coil) and the sample. A Simulink model (Figure 6(a)) of the sample temperature versus time was designed, relating the sample temperature to its
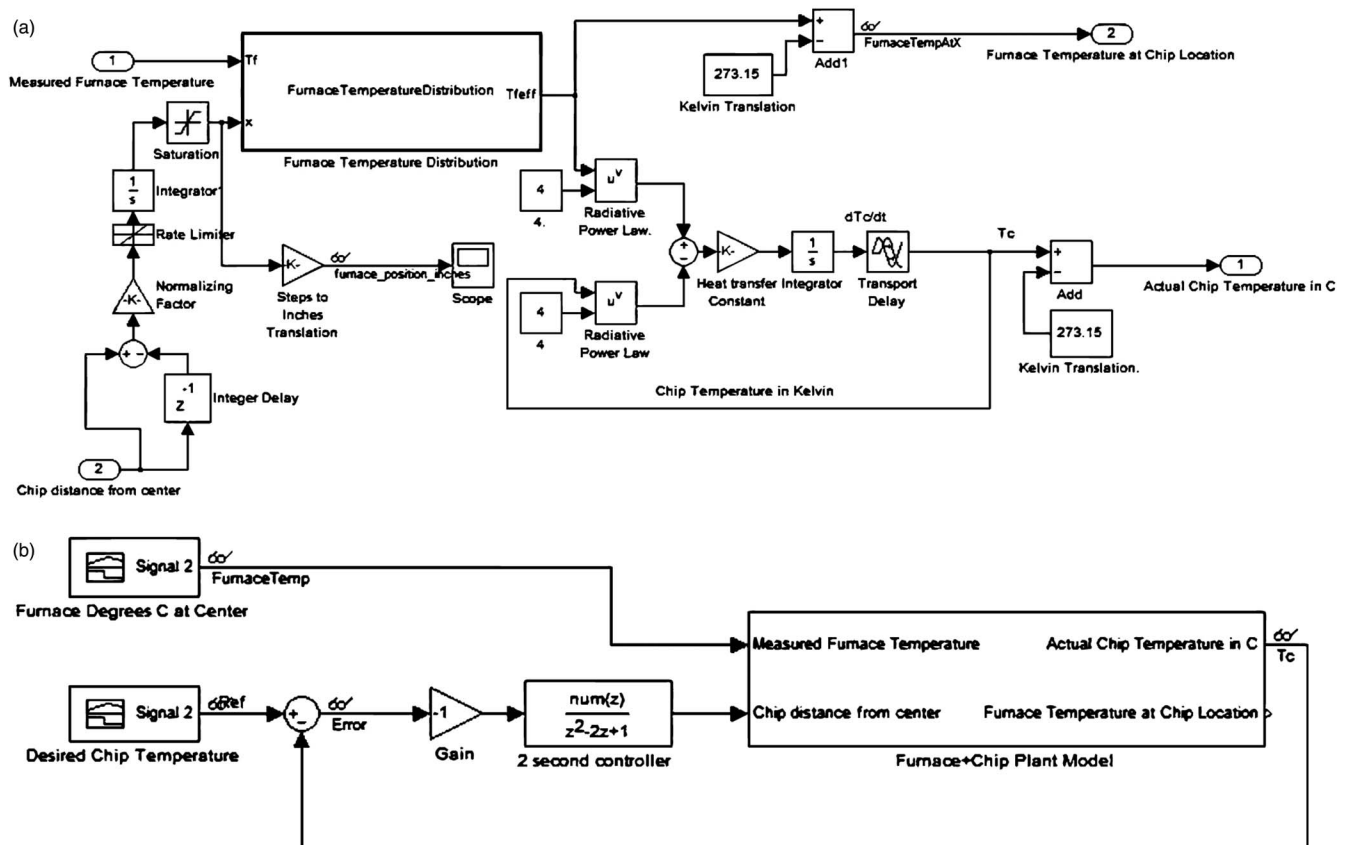
FIG. 6. Architecture for thermal control of the system. (a) System model relating the position and motion of the furnace to the sample temperature. (b) Algorithm used to control the position of the furnace relative to the sample.

position relative to the furnace. The model also included the motion characteristics of the furnace.

Next, a discrete-time PI controller with an additional double-integrator (Eq. (6)) was added to regulate the furnace position, seeking to maintain zero error between the predicted sample temperature and the desired dynamic setpoint:

$$C = K_p + \frac{K_I T}{z - 1} + \frac{K_{I2} T^2}{(z - 1)^2}. \tag{6}$$

Within Eq. (6), K_p is the proportional gain, K_I is the integral gain, K_{I2} is the double integral-gain, and T is the sampling period. This type of controller was selected to account for the slow sampling time (discrete-time), limited by the furnace motion system, while still being capable of achieving a zero steady state error (PI). The double integrator allows the controller to track a ramped input (°C/min) as a set point. We selected a 0.5 Hz sampling time (T) and then manually tuned the control gains.

When in use, the PI controller moves the furnace away from the sample, enabling it to cool rapidly by heat loss to the ambient. As the system cools, it becomes impossible for radiative heat transfer to continue cooling the chip as fast as desired. At this point, the controller has completely retracted the chip out of the furnace and the dominant heat loss mechanism changes from radiation to convection.

III. SYSTEM OPERATION AND VALIDATION

A. Robofurnace operation sequence

In a typical experiment using Robofurnace (Figure 7), the researcher loads boats (which hold the substrate samples in the recessed cavities) into the magazine, closes the door, and inputs a recipe list corresponding to each relevant boat location in the magazine (Figure 7(a)). The researcher then initiates the automated process and Robofurnace performs safety and quality checks. For the CNT growth example discussed later, this includes a baking cycle (850 °C for 30 min in flowing dry air) (Figure 7(b)). The baking cycle cleans the reactor and thereby restores the reactor water vapor and pressure levels to pre-specified baseline values (<120 ppm H_2O, 760 Torr). The quartz transfer arm picks up the boat (with sample) from the load/lock chamber, positions it in the reactor tube for a single experimental run; the reactor is then sealed by a gate valve and flushed with inert gas (i.e., He) (Figure 7(c)). The furnace temperature (up to 1100 °C), furnace position, gas flows, H_2O level, and pressure are all controlled by the recipe during this process. The vision system records changes in the sample as viewed from the forward end of the reactor tube.

After the recipe has concluded, the furnace moves to the forward end of the quartz tube, leaving the sample in view of the surrounding ambient while still sealed in the reactor, allowing the sample to cool rapidly in an inert atmosphere. After cooling, the boat is removed by the transfer arm and returned to the magazine via the load/lock mechanism (Figure 7(e)). Upon completion of the experiment, the researcher is notified electronically and the recorded process data is saved both locally and remotely (via Dropbox and http://www.robofurnace.com). Finally, the results are tweeted (https://twitter.com/Robofurnace), including the researcher's name (optional), Robofurnace machine ID, measured CNT forest height, average growth rate (optional), and an encoded date/time stamp that can be used to download both the raw process data and measurements taken via the vision system from http://www.robofurnace.com (Figure S5 in the supplementary material[20]).

After unloading, the researcher may remove the sample (Figure 7(f)) for further processing and/or characterization. Note that a researcher can add or remove a sample at any time, except for when the transfer arm is in motion. During this period the chamber door will lock for safety. After an experiment is finished and the sample is returned to the magazine, Robofurnace will begin the next experiment in the queue, until all samples in the queue have been processed without the need for the researcher to tend the machine. A video file of this process is available as supplementary material (Video S1) for further clarification.[20]
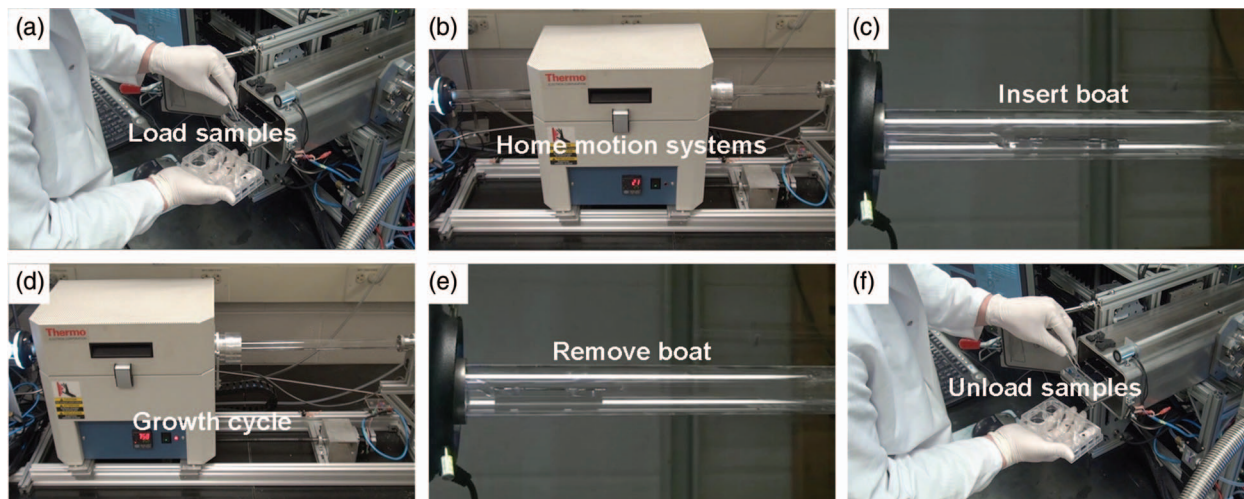
FIG. 7. Motion sequence when Robofurnace processes a single sample. Steps (a)-(f) are sequential steps in one cycle taken from Video S1 (enhanced online) [URL: http://dx.doi.org/10.1063/1.4826275.1].
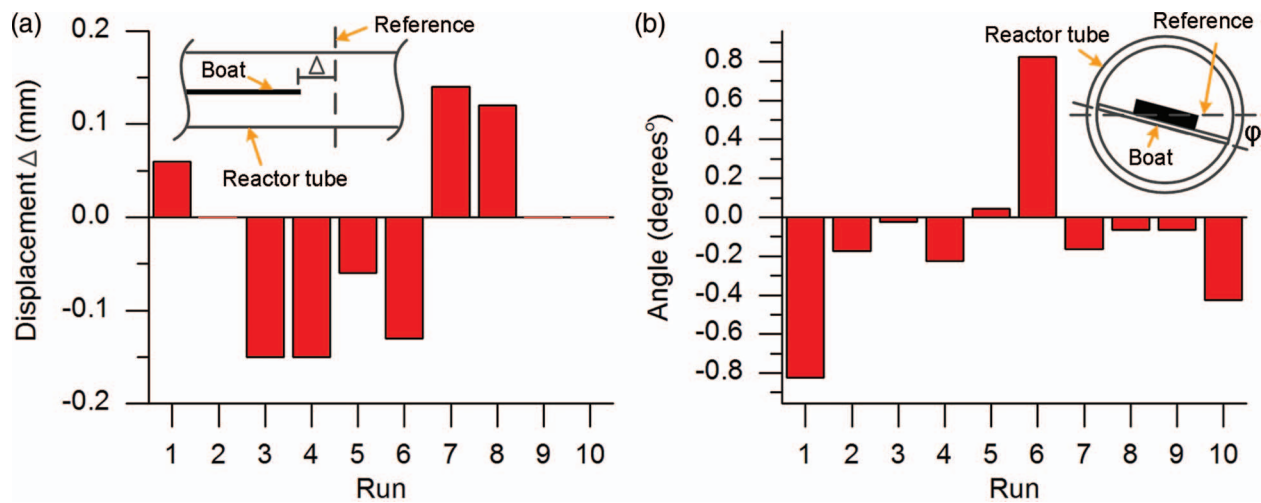
FIG. 8. Measurement of accuracy and repeatability of the pick-and-place operation using the quartz transfer arm and silicon boat. A boat was placed and removed from the reactor tube 10 times. (a) The position of the sample along the reactor tube was measured relative to a reference mark. (b) The angular deviation is shown for the same sample being placed in the tube 10 times, as measured by the angle between the line formed by the boat's contact points with the tube and the horizontal reference axis.

B. Repeatability of sample pick-and-place

The accuracy and repeatability of longitudinal and rotational placement of the boat in the tube furnace was measured, as shown in Figure 8. The same boat was placed in the tube ten times, and the distance from a marked reference location was recorded using a secondary camera (Celestron digital microscope) positioned perpendicular to the reactor tube and the sample. The longitudinal position values deviate from the reference value by a maximum of 150 μm and an average of 0.08 μm, as shown in Figure 8(a). Based on previous studies of the sample position influence on CNT growth, this performance is sufficient to achieve consistent exposure to active gas species along the length of the tube furnace.[11,12] The rotational placement (Figure 8(b)) averages $-0.11°$ with standard deviation of 0.41° from the horizontal axis of the reactor tube. The vision system measurement algorithm accounts for this angular deviation by aligning the measurement coordinate system by edge-finding the bottom edge of the boat.

C. Calibration of the vision system

A vision algorithm (NI Vision Assistant) is used to measure the height of the sample (i.e., the growing CNT forest) during the growth process, from the video provided by the camera. This algorithm finds the top and bottom of the silicon boat, via greyscale threshold edge detection, and assumes the horizontal axis is the line equidistant from the boat top and bottom. The algorithm calculates height by subtracting the top edge of the sample from the bottom edge of the boat (Figure 9(a)).

Vision system calibration was performed with standard silicon wafer samples, resting in the cavity on a boat. First, a reference boat (thickness 500 μm) was inserted into the quartz tube and measured to account for blur outside the DOF. Ten experiments were performed, each with the height measurement averaged over 10 s (Figure 9(b)). The measured height of the Si chip was 475.1 μm with

a standard deviation of 7. 8 μm. This agrees with expected repeatability of the system deviating by one pixel ($\sim$20 μm).

To quantify measurement accuracy, six different Si substrates with CNT films were inserted into the system, and the height measured using the vision system was compared to that measured using a scanning electron microscope (SEM) (Figure 9(c)). The vision system gave values that were consistently greater than via SEM. Figure 9(d) shows an example of measuring CNT forest height using a SEM. The average measurement via the camera was 628 μm with standard deviation of 60 μm. This differs from the SEM by 141 μm on average. The difference between these two measurements methods is accounted for by the way in which each method measures height. The vision system will measure the tallest point on the sample because it relies on projection of the shape, while the SEM method measures the true edge of a sample. It is known that CNT forests taper in height near their edges due to chemical density gradients in the reactor gas flow, which accounts for the difference in measurements. Therefore, the vision system is indicating the maximum height of the forest, based on the projected side view onto the camera.

D. Characterization of heating and cooling control

The ability of Robofurnace to precisely control the heating and cooling rate of the sample, via feedback-controlled motion of the tube furnace, was tested as shown in Figure 10. Robofurnace can control the cooling rate of the sample between 300 °C/min and 1 °C/min.

Figure 10(a) shows a cooling cycle of 15 °C/min, 30 °C/min, and 45 °C/min, achieved by moving the furnace with respect to the sample using the fast cooling controller. Each line is compared to the performance of the simulated controller (Simulink). The error between the linear expected cooling curve and the real temperature is less than the 10 °C specification, with an average deviation of 3.2 °C at 15 °C/min, 2.2 °C at 30 °C/min, and 1.2 °C at 45 °C/min.
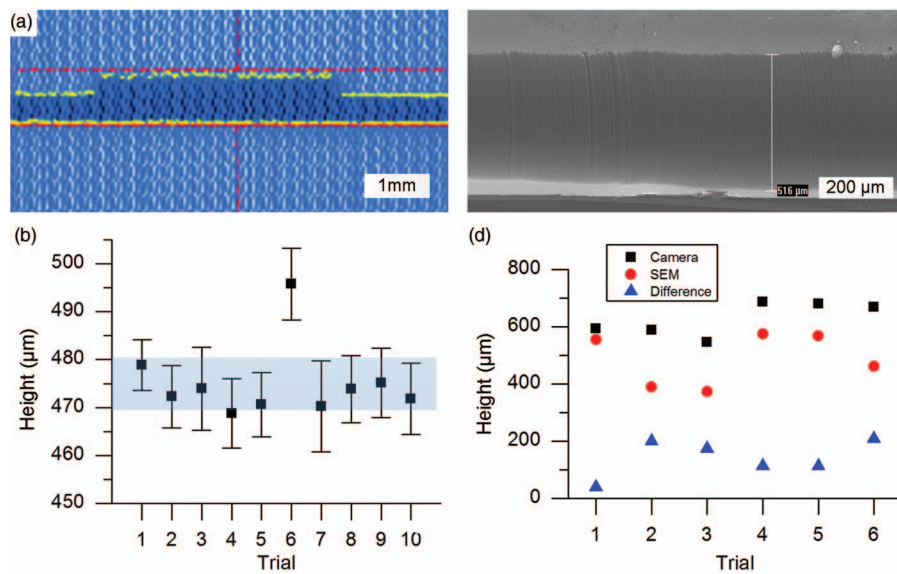
FIG. 9. Repeatability and accuracy of sample height measurement using the vision system to image a CNT forest on a silicon substrate. (a) Side view image with height measurement as seen through the vision system. The red bars indicate the top of the forest and the bottom of the boat. Yellow shows the profile of the forest. (b) Exemplary SEM image of CNT forest. (c) Ten independent measurements taken of this sample, with unloading and re-loading of the sample between measurements. The average height during a 10 s measurement cycle is shown with standard deviations. The blue band represents one standard deviation (5 μm) above and below the 10 trial average height. (d) Comparison of height measurements taken using edge-finding with the vision system and using digital calipers in the SEM.

The maximum and minimum cooling rates obtained without using continuous control of the furnace power and/or position were also determined (Figure 10(b)). The three relevant cases are: moving the furnace to the limit position, so the sample (within the quartz tube) is open to the lab with an external cooling fan on, moving the furnace to the limit position with the fan off, and by turning off the furnace power while keeping the furnace in place. In these cases, the sample cooled from 775 °C to 100 °C in 2.7 min, 7 min, and 140 min, respectively. The first case indicates the maximum cooling rate of the system.

IV. USE OF ROBOFURNACE IN NANOMATERIALS RESEARCH

A. Growth of CNT forests

To demonstrate the first intended use of Robofurnace, we present an exemplary growth of CNT forests based on a procedure outlined by Oliver and Polsen *et al.*[12] The CNT forest growth recipe, including states of the machine at each stage of growth, is shown in Table V. After insertion of the boat (with sample) into the reactor tube, the reactor is purged with He and then He/H$_2$. Then, the furnace is heated to the
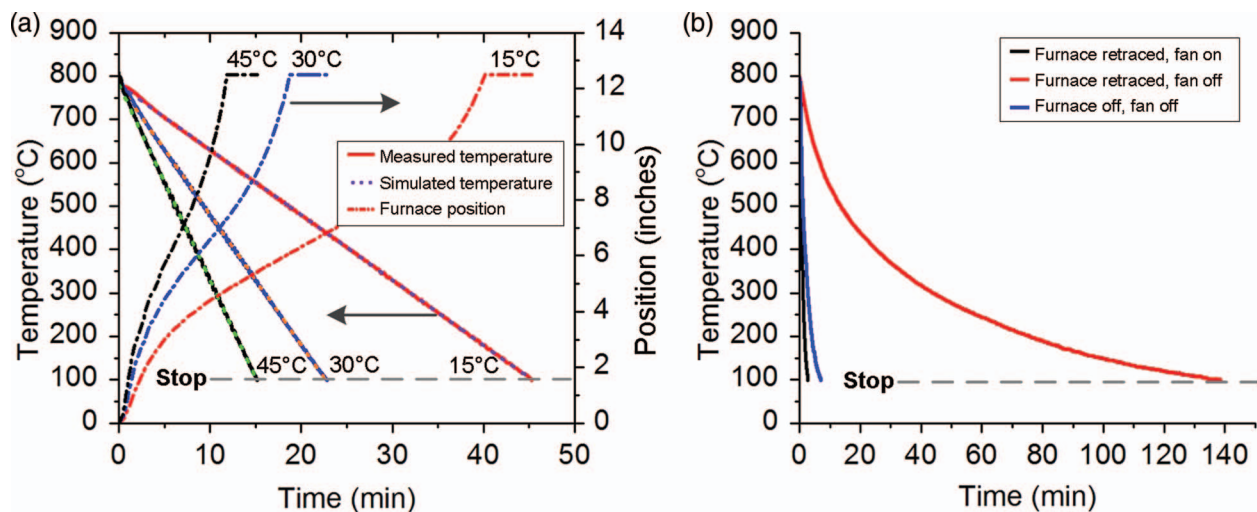
FIG. 10. Characterization of the thermal control system for sample cooling. (a) shows the sample temperature cooling at 15 °C/min, 30 °C/min, and 45 °C/min compared to predicted values. (b) Temperature versus time when the furnace is on the sample and hot, retracted off the sample, and retracted off the sample with a fan turned on, representing the limiting rates of cooling when the control algorithm is not utilized.

TABLE V. Typical carbon nanotube experimental recipe.

Time (min)	He	H$_2$	C$_2$H$_4$	Air	Temperature (°C)	Furnace position (mm)	Pressure (Torr)	Gate valve	Camera	Arm	Magazine	Boat
1	100	0	0	0	Off	0	760	Closed	Off	Home	Home	Out
1	100	0	0	0	Off	280	760	Closed	Off	Home	Home	Out
10	0	0	0	100	850	280	760	Closed	Off	Home	Home	Out
20	0	0	0	100	850	280	760	Closed	Off	Home	Home	Out
5	100	0	0	0	25	280	760	Closed	Off	Home	Home	Out
1	100	0	0	0	25	0	760	Closed	Off	Home	Chip #1	Out
1	100	0	0	0	25	0	760	Closed	Off	Chip	Chip #1	Out
1	100	0	0	0	25	0	760	Closed	Off	Home	Home	Out
1	100	0	0	0	25	0	760	Open	Off	Growth	Home	In
1	100	0	0	0	25	0	760	Closed	Off	Home	Home	In
1	100	0	0	0	25	280	760	Closed	Off	Home	Home	In
5	400	100	100	0	25	280	760	Closed	Off	Home	Home	In
5	100	0	0	0	25	280	760	Closed	Off	Home	Home	In
5	400	100	0	0	25	280	760	Closed	Off	Home	Home	In
10	400	100	0	0	775	280	760	Closed	Off	Home	Home	In
10	400	100	0	0	775	280	760	Closed	Off	Home	Home	In
10	400	100	100	0	775	280	760	Closed	On	Home	Home	In
5	100	0	0	0	25	280	760	Closed	On	Home	Home	In
1	100	0	0	0	25	0	760	Open	Off	Growth	Home	In
1	100	0	0	0	25	0	760	Closed	Off	Home	Chip #1	Out
1	100	0	0	0	25	0	760	Closed	Off	Home	Home	Out
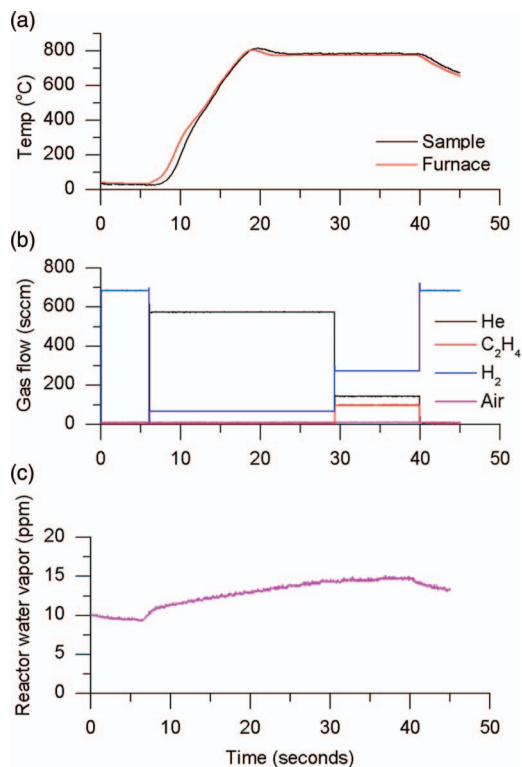
FIG. 11. Real-time process data recorded by the system during synthesis of a CNT forest. (a) Furnace temperature (built-in control thermocouple in heating coil) and sample temperature (thermocouple in contact with furnace tube) versus time. (b) Input flow rate of each gas. (c) Moisture level of input gas flow, measured using hygrometer upstream of reactor at position shown in Figure 1.

setpoint (linear ramp). During this step, the thin film catalyst (Fe) is annealed and dewets from the Si substrate, forming nanoparticles. After annealing the carbon precursor, ethylene (C$_2$H$_4$) is added to the input gas stream.[21] The ethylene decomposes into favorable and unfavorable gas species, which thermally activates in the hot furnace and reacts with the substrate, resulting in a "forest" of aligned CNTs collectively growing upward form the substrate.[21] After 10 min the flow of C$_2$H$_4$ is terminated and the CNTs stop growing. The real-time data recorded during an experiment with this recipe are shown in Figure 11. The reactor moisture level (Figure 11(c)), as measured by a hygrometer, varies between 10 and 15 ppm throughout the experiment. This is a baseline value for the reactor after purging. In this experiment the pressure is atmospheric and is not controlled by the system.

Robofurnace also uses the vision system, as previously described, to record the height of the CNT forest. Figure 12 shows kinetic data derived from the video, including the CNT height versus time, the growth rate, surface traces obtained by the edge detection algorithm, and raw images before and after the process.[22] The software estimates the instantaneous CNT growth rate as the rate of change in substrate thickness between consecutive video frames.[23,24] Surface profile tracing enables the experimenter to measure the profile of the film as it develops with respect to time (Figure 12(d)). This is useful to terminate the growth at a pre-specified height or measure the abrupt growth termination due to CNT forests self-limiting behavior.[24]
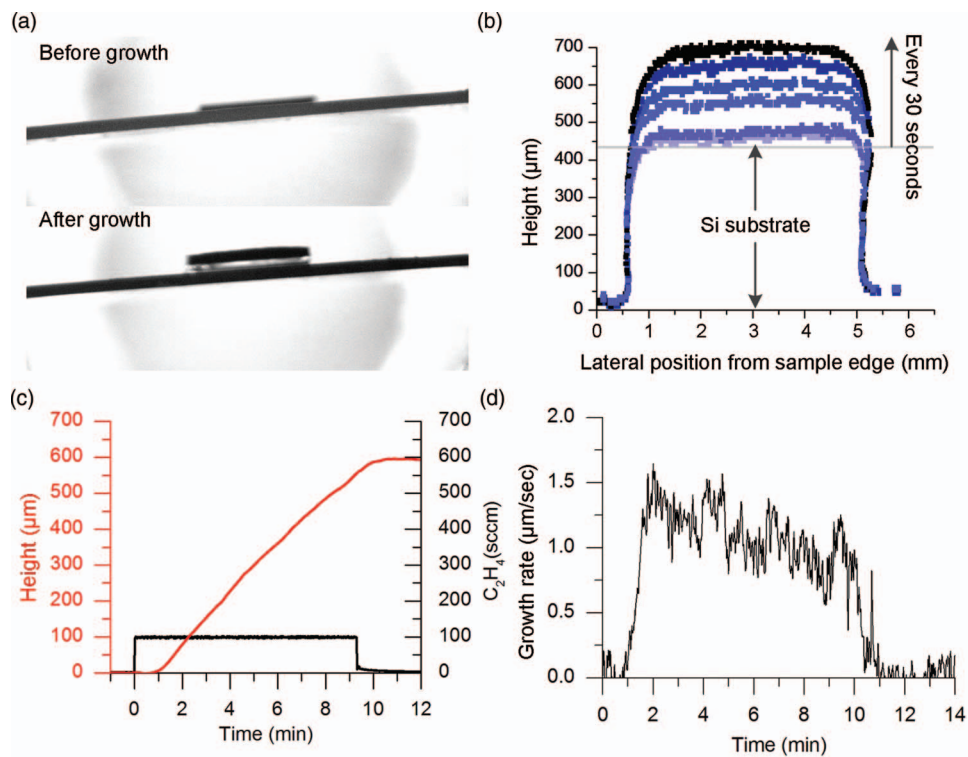
FIG. 12. Use of the vision system for real-time analysis of CNT growth kinetics. (a) A view of the substrate before and after the experiment. The CNT forest can be seen as a dark layer on top of the Si substrate. (b) A profile of the CNT film is plotted every 30 s (for a different experiment). (c) During the synthesis step in which a carbon source is introduced the vision system measures the thickness of a CNT film in μm. (d) The rate of growth of the film in μm/s, which first increases rapidly to a maximum, then gradually decays, and then abruptly stops after 10 min when the growth step concludes.

B. Reduced process variation due to automation of CVD

In a recent study using a manual tube furnace, we found that CNT forest height and density is prone to substantial variation due to ambient factors and different researcher habits; therefore, a goal of developing Robofurnace was to enable reduced process variation via automation. Specifically, fluctuations in ambient humidity affect the density and diameter of the catalyst nanoparticles formed during annealing and influence the gas phase reactions in the furnace,[12] resulting in CNT density and growth rate variation.

To combat this variation, Robofurnace uses stainless steel tubing with a hygrometer to monitor and adjust the reactor water vapor level to within 50 ppm H_2O, which gives 100-fold less variability in the moisture level inside the tube compared to a manual tube furnace with PTFE tubing. Robofurnace also isolates the samples from the ambient lab conditions via use of the load/lock chamber, which is independently purged while the furnace is sealed. The transfer arm controls the sample position in the reactor tube. Last, the gas delivery system and furnace PID controller tightly control temperature and gas flow.

Therefore, we sought to investigate how Robofurnace can reduce variability of CNT forest height and density by performing 26 identical CNT growth experiments (Figure 13). The results using Robofurnace had a coefficient of variation of CNT film height and density of 15% and 23%, respectively, compared to 31% and 63% for a manual process using a non-automated tube furnace. This represents a 50% and 62% re-

duction in the coefficient of variation for height and density, respectively.

We claim automated control contributes to reduced variability compared to manually setting each process parameter. In addition, continual improvement of measurement accuracy adds strength to conclusions derived from experimentation. However, there is still remaining variation in this process, and it may be necessary to tune the process parameters (gas mixture, temperature, catalyst, and reactor humidity) to maximize film uniformity. In order to discover the remaining factors contributing to growth variation, further study is needed of other contaminants (e.g., oxygen) in the reactant mixture, the influence of inherent moisture changes during both annealing and growth, the influence of reactor pressure, both the accuracy and repeatability of gas flow control, and the effects of potential trace metal contaminants in the thin film catalyst. Nevertheless, via Robofurnace we show that automation provides a versatile platform to perform parametric studies of CNT forest growth, for reduction of variation and improvement of CNT forest properties.

C. Use of automated dynamic CVD to grow higher density CNT forests

Last, we demonstrate use of Robofurnace to optimize and discover a new recipe that gives CNT forests with higher density. Achieving high density CNT forests (i.e., a high density of CNTs per unit area) is an important challenge in this
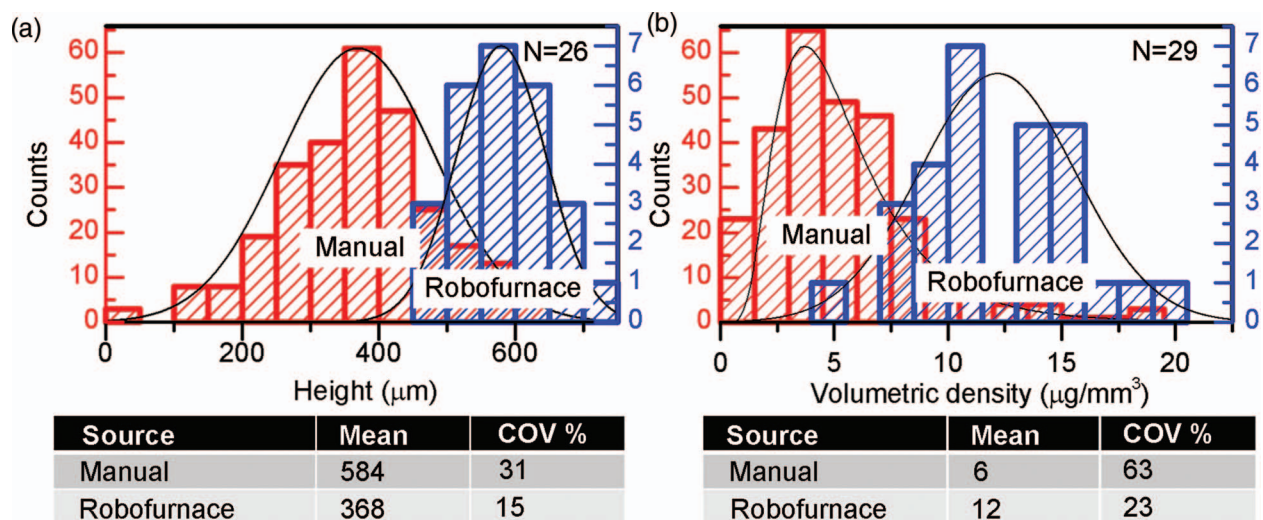
FIG. 13. A comparison CNT forest growth statistics obtained using a standard manual tube furnace and an automated tube furnace under the same conditions, via histograms of (a) height and (b) volumetric density. The manual growth study and the analysis of variation are described by Oliver *et al.*[12] Reprinted with permission from C. Ryan Oliver, E. S. Polsen, E. R. Meshot, S. Tawfick, S. J. Park, M. Bedewy, and A. J. Hart, ACS Nano **7**, 3565 (2013). Copyright 2013 American Chemical Society.
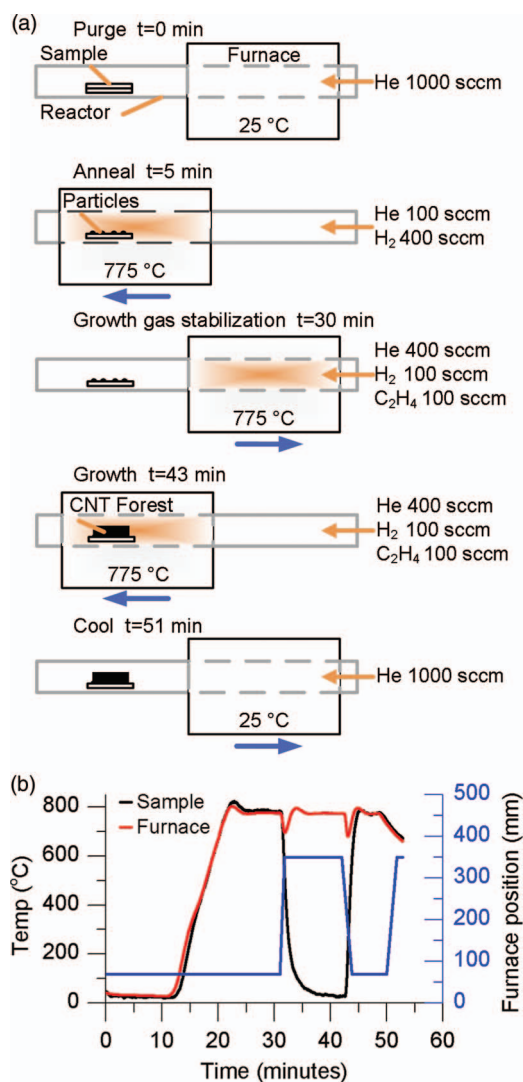
FIG. 14. (a) Schematic of the dynamic growth recipe with time. (b) Recorded processing parameters for dynamic recipe showing temperature of sample, furnace, and position of the furnace against time.

field[25–28] and can be directly related to bulk mechanical,[29] thermal,[30] and electrical[31, 32] properties of CNT assemblies.

We hypothesized that rapid introduction of the sample into the hot furnace containing a stable hydrocarbon mixture would increase the density of CNTs in the forest by increasing the activation percentage of the catalyst particles and enable decoupled understanding of the influence of the annealing and growth recipe parameters. Therefore, we chose to explore a "dynamic" recipe (Table SI in the supplementary material[20]), whereby Robofurnace moves the position of the furnace with time (Figure 14), decoupling the change in the gas atmosphere from the temperature of the sample. After annealing in He/H$_2$ (100/400 sccm), the furnace is moved away from the sample. The sample is allowed to cool while remaining in the tube. At the same time, the flow compositions change to 400/100/100 sccm He/H$_2$/C$_2$H$_4$ and the flow is allowed to stabilize for 3 minutes. Next, the furnace (still hot) moves back onto the sample quickly heating it to the reaction temperature.

Six experiments were performed to explore the relationship between the furnace setpoint temperature (750 °C, 775 °C, 800 °C) and the position of the sample relative to the center of the furnace (dynamic vs. static), which controls activity of the gas via residence time in the tube before reaching the sample. Measurements from this experiment are shown in Figure 15 and recorded process parameters are in Figure S6 in the supplementary material.[20] We found that optimizing a dynamic recipe with a furnace temperature of 750 °C achieved nearly a 6-fold higher (7.44 × 10^{-2} mg/mm^3 vs. 1.25 × 10^{-2} mg/mm^3) volumetric density on average than a static recipe, performed using Robofurnace, as described in Table V. When compared to the manual tube furnace, the automated system yielded a volumetric density that was 14-fold higher. Therefore, by using Robofurnace as an optimization tool, we demonstrated an order of magnitude improvement in density of CNT forest over previously reported values in the same laboratory.
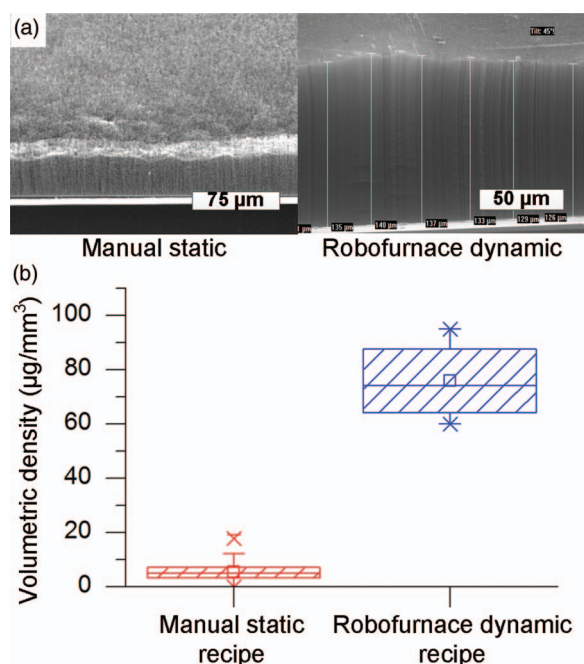
FIG. 15. (a) SEM images of a forest from a manual furnace and using Robofurnace. (b) A comparison of the volumetric density of CNT forests synthesized using a manual furnace static recipe and after optimization using Robofurnace dynamic recipe at 750 °C.

V. CONCLUSION

Robofurnace is a semi-automated CVD system, built around a standard horizontal tube furnace, which enables synthesis of materials on centimeter-scale substrates. The system features automated insertion and removal of samples into a 10 slot magazine, and has an asynchronous multi-user software interface and queue. Coupled with a machine vision system and motorized furnace, Robofurnace enables repeatable and automated exploration of large processing parameter spaces. Robofurnace requires user touch time of less than 1 h per day and can perform 16 or more CVD experiments in a 24 h period. This compares to 2–4 experiments tending to a manual system during a normal workday.

We demonstrated that Robofurnace can achieve CNT forest synthesis with improved consistency compared to a manual CVD system and can rapidly identify new recipes for increased CNT forest density. In the future, Robofurnace could be coupled with artificial intelligence in order to efficiently search larger sample spaces and optimize recipes to achieve target material properties. Moreover, the accessibility of process recipes, metrology data, and characterization results via the data cloud could enable systems in different labs to communicate and solve collaborative tasks defined both by humans and machines.

ACKNOWLEDGMENTS

[1] S. Curtarolo, G. L. W. Hart, M. B. Nardelli, N. Mingo, S. Sanvito, and O. Levy, Nature Mater. **12**, 191 (2013).

[2] *Fact Sheet: Progress on Materials Genome Initiative* (O. o. S. a. T. Policy, Washington, DC, 2012).

[3] F. J. del Campo, J. Garcia-Cespedes, F. X. Munoz, and E. Bertran, Electrochem. Commun. **10**, 1242 (2008).

[4] S. Esconjauregui, M. Fouquet, B. C. Bayer, C. Ducati, R. Smajda, S. Hofmann, and J. Robertson, ACS Nano **4**, 7431 (2010).

[5] W. Q. Fu, L. Liu, K. L. Jiang, Q. Q. Li, and S. S. Fan, Carbon **48**, 1876 (2010).

[6] H. Huang, C. H. Liu, Y. Wu, and S. S. Fan, Adv. Mater. **17**, 1652 (2005).

[7] A. M. Marconnett, N. Yamamoto, M. A. Panzer, B. L. Wardle, and K. E. Goodson, ACS Nano **5**, 4818 (2011).

[8] S. Tawfick, K. O'Brien, and A. J. Hart, Small **5**, 2467 (2009).

[9] K. S. Novoselov, V. I. Fal'ko, L. Colombo, P. R. Gellert, M. G. Schwab, and K. Kim, Nature (London) **490**, 192 (2012).

[10] D. N. Futaba, K. Hata, T. Yamada, K. Mizuno, M. Yumura, and S. Iijima, Phys. Rev. Lett. **95**, 056104 (2005).

[11] G. Li, S. Chakrabarti, M. Schulz, and V. Shanov, Carbon **48**, 2111 (2010).

[12] C. Ryan Oliver, E. S. Polsen, E. R. Meshot, S. Tawfick, S. J. Park, M. Bedewy, and A. J. Hart, ACS Nano **7**, 3565 (2013).

[13] B. G. Buchanan and E. A. Feigenbaum, Artif. Intell. **11**, 5 (1978).

[14] R. E. Carhart, S. M. Johnson, D. H. Smith, B. G. Buchanan, R. G. Dromey, and J. Lederberg, ACS Symp. Ser. **19**, 192 (1975).

[15] R. K. Lindsay, B. G. Buchanan, E. A. Feigenbaum, and J. Lederberg, Artif. Intell. **61**, 209 (1993).

[16] D. K. Agrafiotis, V. S. Lobanov, and F. R. Salemme, Nat. Rev. Drug Discovery **1**, 337 (2002).

[17] S. Semancik, R. E. Cavicchi, M. C. Wheeler, J. E. Tiffany, G. E. Poirier, R. M. Walton, J. S. Suehle, B. Panchapakesan, and D. L. DeVoe, Sens. Actuators B **77**, 579 (2001).

[18] G. D. Nessim, A. Al-Obeidi, H. Grisaru, E. S. Polsen, C. R. Oliver, T. Zimrin, A. J. Hart, D. Aurbach, and C. V. Thompson, Carbon **50**, 4002 (2012).

[19] J. M. Geary, *Introduction to Lens Design: With Practical ZEMAX Examples* (Willmann-Bell, Incorporated, Richmond, 2002).

[20] See supplementary material at http://dx.doi.org/10.1063/1.4826275 for video demonstrations using Robofurnace.

[21] D. L. Plata, E. R. Meshot, C. M. Reddy, A. J. Hart, and P. M. Gschwend, ACS Nano **4**, 7185 (2010).

[22] M. Stadermann, S. P. Sherlock, J. B. In, F. Fornasiero, H. G. Park, A. B. Artyukhin, Y. M. Wang, J. J. De Yoreo, C. P. Grigoropoulos, O. Bakajin, A. A. Chernov, and A. Noy, Nano Lett. **9**, 738 (2009).

[23] M. Bedewy, E. R. Meshot, H. C. Guo, E. A. Verploegen, W. Lu, and A. J. Hart, J. Phys. Chem. C **113**, 20576 (2009).

[24] E. R. Meshot and A. J. Hart, Appl. Phys. Lett. **92**, 113107 (2008).

[25] M. Bedewy and A. J. Hart, Nanoscale **5**, 2928 (2013).

[26] M. Bedewy, E. R. Meshot, M. J. Reinker, and A. J. Hart, ACS Nano **5**, 8974 (2011).

[27] E. S. Polsen, M. Bedewy, and A. J. Hart, Small **15**, 5264 (2013).

[28] G. F. Zhong, J. H. Warner, M. Fouquet, A. W. Robertson, B. A. Chen, and J. Robertson, ACS Nano **6**, 2893 (2012).

[29] J. N. Coleman, U. Khan, W. J. Blau, and Y. K. Gun'ko, Carbon **44**, 1624 (2006).

[30] R. S. Prasher, X. J. Hu, Y. Chalopin, N. Mingo, K. Lofgreen, S. Volz, F. Cleri, and P. Keblinski, Phys. Rev. Lett. **102**, 105901 (2009).

[31] P. N. Nirmalraj, P. E. Lyons, S. De, J. N. Coleman, and J. J. Boland, Nano Lett. **9**, 3890 (2009).

[32] A. E. Islam, F. Du, X. N. Ho, S. H. Jin, S. Dunham, and J. A. Rogers, J. Appl. Phys. **111**, 054511 (2012).